



Novel non-destructive authentication of nine *Dendrobium* species using residual convolutional neural network relying on plant images and FT-NIR spectral information

Yulin Xu ^{a,b,1}, Lian Li ^{a,c,1}, Yuanzhong Wang ^{a,*}, Qiang Hu ^{a,*}

^a Medicinal Plants Research Institute, Yunnan Academy of Agricultural Sciences, Kunming 650200, PR China

^b School of Ecology and Environmental Science, Yunnan University, Kunming, 650091, PR China

^c College of Fundamental Medicine, Chengdu University of Traditional Chinese Medicine, Chengdu, 611137, PR China



ARTICLE INFO

Keywords:

Medicinal plant

Dendrobium

Machine learning

Residual neural network

Non-destructive authentication

ABSTRACT

Various *Dendrobium* species used as traditional Chinese medicine have similar appearances but different bioactive component, with significant differences in medicinal and economic values. Many commercially available herbal medicines, including *Dendrobium* are usually powdered, and commercial fraud by adulterating cheap species in the supply chain often occurs. Therefore, it is necessary to develop accurate and feasible authentication methods for herbal medicines. Currently, non-destructive testing and analysis are gradually becoming a hot issue in various industries. This study attempts to use machine learning techniques for non-destructive combination authentication of different *Dendrobium* species based on plant photographs (SONY) and Fourier transform near-infrared spectroscopy (FT-NIR). Simultaneously validated the ability of the residual neural network (ResNet) and support vector machine (SVM) models to extract and recognize features from different preprocessed datasets. The results showed that *Dendrobium officinale* had the highest absorbance followed by *Dendrobium thyrsiflorum* and *Dendrobium crepidatum* had the lowest. When the weight decay coefficient λ of the deep learning model based on ResNet is 0.0001 and the learning rate is 0.01, it can identify up to 100 % of *Dendrobium* species. ResNet recognizes feature information of plant images with an accuracy of up to 88.2 %. Using flower parts with more recognised features or controlling the consistency of the background may improve recognition accuracy. The dataset of synchronized two-dimensional correlation spectroscopy (2DCOS) does not require preprocessing, and the ResNet model can accurately and quickly extract recognition features. Deep learning models based on ResNet have absolute advantages over traditional SVM models in terms of accuracy and recognition speed. The analytical method proposed in this study may provide new ideas for non-destructive identification of similar species, genuine and fake products, pest and disease characteristics in the field of agriculture.

1. Introduction

Dendrobium is one of the largest genera of orchids and among the largest genera of angiosperms. There are about 1500 species worldwide, primarily found in tropical, subtropical regions, and Oceania in Southeast Asia [1]. Most *Dendrobium* species are "attached to trees" and have important medicinal and ornamental values [1]. China is the northern border area of *Dendrobium* with abundant resources. The Flora of China reports approximately 78 *Dendrobium* species in China, with 60 species specifically found in Yunnan province. In China, Yunnan is the region with the largest number of *Dendrobium* species.

Significant variations exist in the chemical composition, content, and bioactivity among various *Dendrobium* species. Xing et al. indicated higher coumarin content in *D. densiflorum* and *D. thyrsiflorum* compared to other species [2]. Gu et al. identified that all six species of *Dendrobium* contain eight main metabolites in comparable amounts [3]. It may also represent a universal protocol for the authentication and quality assessment of medicinal herbs. As the chemical components in different species of *Dendrobium* are different, they can directly affect the relevant clinical therapeutic effects [4]. Commercially available *Dendrobium* is usually powdered, and unscrupulous traders usually pass off the cheap as the expensive. Therefore, it is necessary to trace the labeling

* Corresponding authors.

E-mail addresses: boletus@126.com (Y. Wang), huqiang@yaas.org.cn (Q. Hu).

¹ These authors contributed equally to this work.

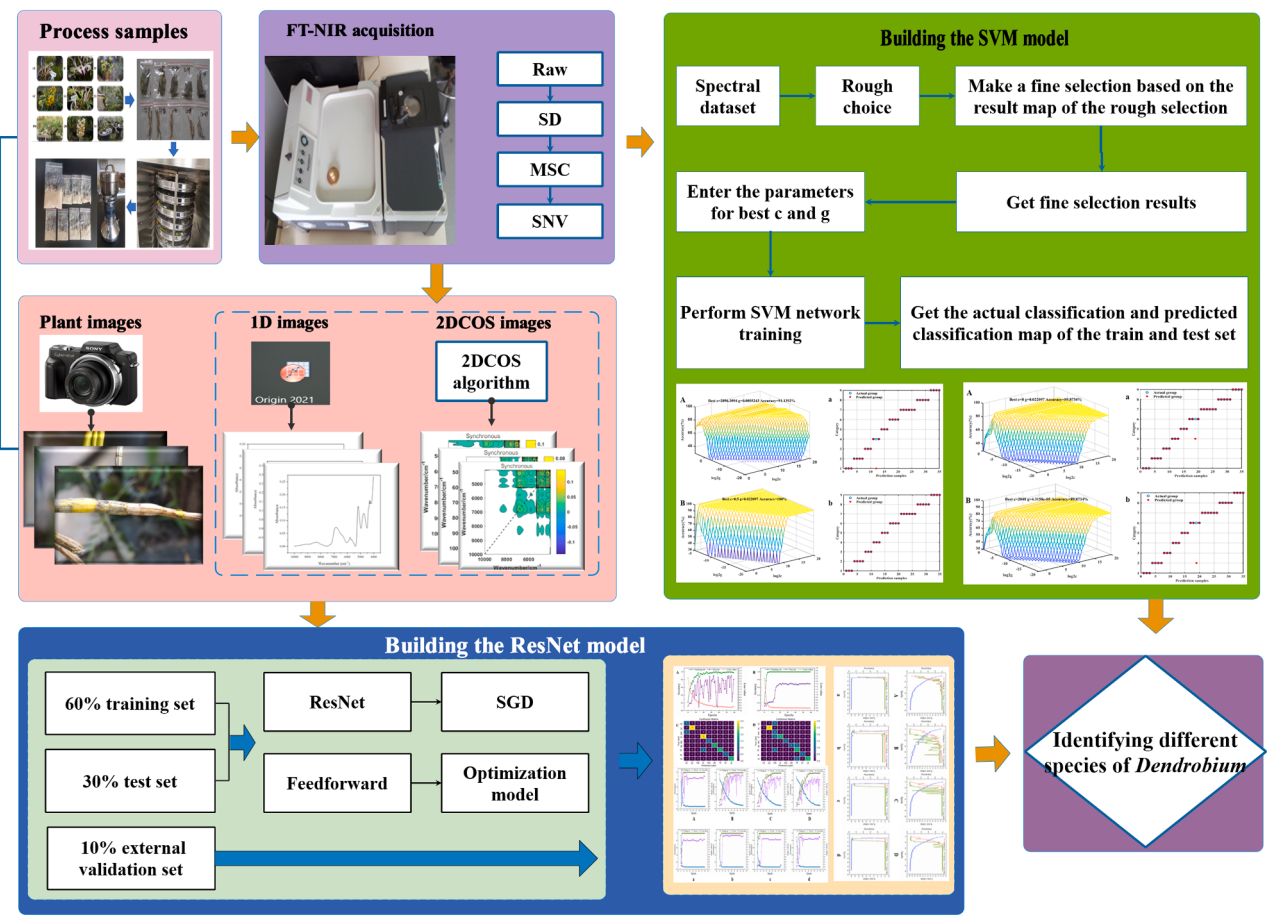


Fig. 1. The flowchart of the whole study.

information and the real information of the products to ensure the validity and safety for food and medicinal use.

With the development of detection and analysis technology, non-destructive and efficient near-infrared spectroscopy (NIR) is a common technique to achieve this [5,6]. Fourier transform near-infrared spectroscopy (FT-NIR) is simple to operate, does not destroy the microstructure of the sample, and can comprehensively describe its information characteristics [7]. The FT-NIR has been widely used for quality authentication of herbs and spices. The analysis of FT-NIR focuses on the extraction of feature information and the establishment of a multivariate statistical model for comprehensive analysis [8,9]. Models such as principal component analysis (PCA) [10], partial least squares discriminant analysis (PLS-DA), and support vector machines (SVM) [11], etc. are the most commonly used multivariate statistical analysis methods. However, despite their popularity and continuous improvement, the amount of spectral information they can extract is limited [12]. Traditional machine learning requires tedious preprocessing and feature extraction, making it difficult to achieve fast identification. In recent years, deep learning (DL) techniques have been widely used in many fields of remote sensing, including image and voice recognition [13]. To underscore the importance of DL in agricultural regions compared to traditional machine learning, a case demonstrates the development and recent trends of hyperspectral systems in rice cultivation [14]. The future of agriculture depends heavily on the adoption of these new technologies [11]. Convolutional neural network (CNN), as one of the deep learning algorithms, is widely used in the image recognition [15]. With the improvement of numerical computing efficiency, its massive potential for processing digital image data has been fully discovered and tapped [16]. Then, VGG, GoogLeNet, and residual neural network (ResNet) were also proposed one after another. ResNet

won the “imageNet large-scale visual recognition challenge” in 2015, which has good convergence and accuracy [17]. The main contribution of the residual neural network is the discovery of “Degradation” and the invention of “Shortcut connection” for the degradation phenomenon, which eliminates the difficulty of training neural networks with excessive depth [18]. Based on the advantages of ResNet, it will provide practical reference and new thinking for plant species detection. Akter and Hosen proposed an automatic classification system for medicinal plants on CNN, and the accuracy rate of the recognition method was around 71.3 % [19]. The reason for low accuracy may be that not enough identifying features were extracted from the leaves of the medicinal plant and adding other parts of the plant in combination with the leaves may give better results.

In previous research, researchers often convert one-dimensional (1D) spectral data into two-dimensional correlation spectroscopy (2DCOS) images, and then directly combine the ResNet model to solve various agricultural problems, such as species identification [20], geographic traceability [21], and determination of harvesting periods [9]. Compared to 1D spectral images, 2DCOS enriches the spectral information of chemical molecules and functional groups, and is more suitable for identification using two-dimensional digital image processing methods [22]. At present, 2DCOS technology has been applied to detect the adulteration and geographical traceability of certain foods and herbs with CNN. However, a lot of work is required in the process of processing the sample, such as collecting, cleaning, powdering, scanning infrared, etc. Extensive literature demonstrates that direct use of plant images for identification can complement this shortcoming. A digital camera (Canon 660D) was used to collect 8911 images of rice leaf disease as a dataset and combined with DL and SVM for recognition [23]. However, using CNN models requires a large amount of image information for

training in order to obtain better recognition results. Gopal et al. were committed to using medical plants leaf images for classification, with a classification accuracy of 92 % [24]. Although direct acquisition of plant images reduces the amount of work involved in processing samples, the images used for modeling are very demanding and rarely reach 100 % accuracy. Therefore, combining photographic information of plants with non-destructive chemical information may be a better choice.

This study compare and analyze the features and advantages of different datasets by combining traditional models (SVM) and ResNet, and select methods suitable for non-destructive and fast identification of *Dendrobium* species. The flowchart in this study is shown in Fig. 1. Firstly, images combined with ResNet model were used to identify nine species of *Dendrobium*. Input images include one-dimensional and two-dimensional FT-NIR images (Raw, Second derivative, Standard Normal Variable, Multiplicative Scattering Correction) and plant images. Secondly, the effect of different convolutional layers (16 and 32) on the result of the ResNet model was compared. Thirdly, the SVM models were built using the FT-NIR information to compare the advantages of the ResNet models. Based on the above, the most suitable model was selected. This study provides FT-NIR characteristics interpretation and non-destructive rapid identification of 9 *Dendrobium* species, and can also provide a reference for non-destructive identification of similar species, genuine and fake products, pest and disease characteristics in the field of agriculture.

2. Materials and Methods

2.1. Collection of plant sample

In 2022, we collected and photographed nine *Dendrobium* species in Yuxi city, Yunnan Province ($102^{\circ}32'41.112''$ E, $24^{\circ}21'19.74''$ N), and detailed sample information is shown in Figure S1 and Table S1. The samples were identified by Professor Hengyu Huang (Institute of the Traditional Chinese Medicine, Yunnan University of Traditional Chinese Medicine, Kunming, China). The whole *Dendrobium* plants were separated according to different parts (stems and leaves). The fresh stems were dried to constant weight at 45°C , pulverized by a high-speed pulverizer (Tianjin Huixin Machinery Co., Ltd., Tianjin), and passed through an 80-mesh stainless steel sieve. The powder was then placed in a transparent PE-sealed bag and stored in a cool, dry and dark room.

2.2. Acquire FT-NIR Spectra

The Antaris II spectrometer (Thermo Fisher Scientific Inc., Waltham, MA, USA) is equipped with a diffuse reflectance module to detect samples in this mode. The FT-NIR spectral data was collected in 2022. The spectral scanning interval was 1.95 cm^{-1} and the scanning range was $10,000\text{--}4000\text{ cm}^{-1}$ with the resolution of 8 cm^{-1} . Weigh about 20 g of each sample into a sample cup, scan 64 times cumulatively, the spectral ordinate was measured using $\log(1/\text{reflectance})$ and repeated 3 times. The average spectrum for 3 times was used as the final analysis data. In order to exclude the interference of sampling volume and laboratory conditions (air and moisture), the laboratory temperature and humidity were controlled at 25°C and 30 %.

2.3. Data preprocessing

Spectral preprocessing corrects for artifacts and removes noise to enhance the spectral feature information of interest. The use of inappropriate preprocessing technologies may negatively affect the model [25]. Commonly used preprocessing techniques are as follows according to the characteristics and applicability, which will select these methods for this study: (1) Standard normal variate (SNV) correction and multiplicative scatter correction (MSC) were rely on baseline correction and normalization; (2) Derivative processing improves the spectral resolution and obtains spectral information of overlapping peaks, especially

second-order derivatives (SD). Second-order derivative transformation using a 15-point Savitzky-Golay smoothing filter to improve spectral resolution while minimising noise amplification. Subsequently, compare the impact of preprocessing techniques on classification models by comparing unprocessed and preprocessed data.

2.4. Exploratory analysis

Principal component analysis (PCA), the principle is recombined the original variables into a new set of several comprehensive variables that are independent about each other. At the same time, according to actual needs, several important components can be extracted from it to reflect as much information as possible from the original variable. The PCA is a downscaling and exploratory unsupervised learning method that is widely used to visualize data. In this study, SIMCA 14.1 software was used for analysis, with the first two principal components (PC1 and PC2) to reflect the clustering trend of the samples.

2.5. The different category spectral images acquisition

2.5.1. Plant images

In previous studies, scanners or digital cameras were used to obtain leaf images for identification [23]. In this study, to preserve the original form of the plant, we took pictures of 10 or more stems of each species with a camera (SONY) at the base. It is worth noting that the parameters of the camera are set to the macro mode in order to try to avoid the influence of the cluttered background on the later modeling. Then, the plant images were stored as JPEG image of the same size as 128×128 pixels for modeling. The detailed images of 9 different *Dendrobium* plants images randomly selected in Figure S2 A. All 191 plant images were randomly selected as training set 116 (60 %), 58 (30 %) as test set, and 17 (10 %) as external validation set.

2.5.2. 1D FT-NIR spectral image acquisition

Obtain one-dimensional (1D) FT-NIR spectral images directly using Origin 2021. Before this, the spectrograms of all samples were converted into a data matrix by SIMCA 14.1 software. To avoid manipulation and other physical errors in the 1D images, the horizontal and vertical coordinate values of each image were set to be the same. The image size is shown in Figure S2 B.

2.5.3. 2DCOS spectral image acquisition

Compared with one-dimensional spectroscopy, two-dimensional correlation spectroscopy (2DCOS) can effectively solve the spectral overlap problem and improve the spectral resolution. In this study, the discrete generalized 2DCOS algorithm is used for the computation [26]. According to Noda's description of the two-dimensional spectrum, the dynamic spectral intensities at variable v are calculated as W , and the t is the external perturbation for the spectrum measured at m steps [27].

$$W(v) = \begin{bmatrix} y(v, t_1) \\ y(v, t_2) \\ y(v, t_3) \\ \vdots \\ y(v, t_n) \end{bmatrix} \quad (1)$$

Therefore, the expression of synchronous two-dimensional correlation intensity between v_1 and v_2 was displayed as $\Phi(v_1, v_2)$.

$$\Phi(v_1, v_2) = \frac{1}{m-1} Y(v_1)^T \cdot W(v_2) \quad (2)$$

Where N is the Hilbert-Noda matrix as defined formula (3).

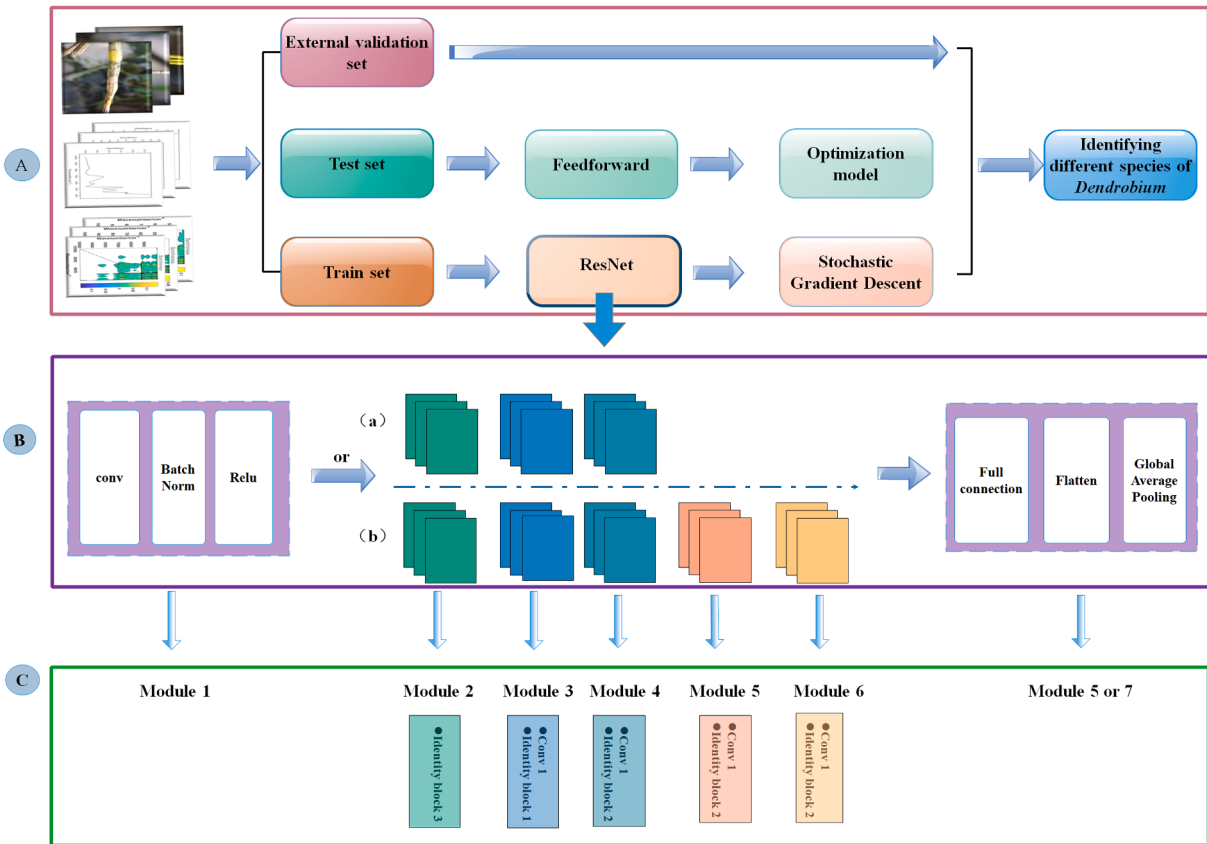


Fig. 2. The flow chart of the ResNet model discrimination strategy. A: The process of classifying different species of *Dendrobium* by inputting three images into ResNet models. B: The structure of the ResNet models, (a) with 16 layers and (b) with 32 layers. C: The composition and number of residual modules.

$$N_{jk} = \begin{cases} 0, & j = k \\ \frac{1}{\pi(k-j)}, & j \neq k \end{cases} \quad (3)$$

In this research, matrix W ($m \times n$) possesses two spectra data ($m = 2$) that the first is the average FT-NIR spectrum and the second is the i th FT-NIR spectrum of each species on *Dendrobium* [28–30]. Finally, the synchronous 2DCOS spectral images were displayed in Figure S2 C and the specific flowchart is shown in Figure S3. For FT-NIR spectrum, all 2DCOS images were randomly selected as training set 68 (60 %), 35 (30 %) as test set and 11 as external validation set (10 %). Based on this, these datasets were used to build residual neural networks to carry out further research.

2.6. Establishment of ResNet model based on images of different categories

Deep learning, as a type of machine learning, is to learn the inherent laws and representation levels of sample data. The information obtained during these learning processes is of great help to the interpretation of data such as text, images, and sounds. Its ultimate goal is to enable machines to have the ability to analyze and learn like humans to recognize data such as words, images, and sounds. DL is a complex machine learning algorithm, that can achieve results in speech and image recognition far beyond previous related technologies. Convolutional neural network is one of the representative algorithms of deep learning and is widely used in contemporary artificial intelligence research [17]. In this work, the MXNet was chosen as the deep learning framework, a quad-core 8 G ECS cloud server with Python and Anaconda installed was adopted as the data processing hardware platform. Additionally, MxBoard for training process visualization was installed.

ResNet, as one new type of CNN, the residual module is introduced into the deep neural network, the redundant network structure is discarded, and the operation speed is accelerated to a certain extent, which solves the gradient disappearance and network degradation problems of the traditional neural network [31]. As shown in Figure S4, the input of plain network is x , while the output is $H(x)$. However, the input x is directly transmitted to the output in the residual convolution neural network and the objective result is $F(x) = H(x)-x$. As the depth of the network increases of CNN, the gradient vanishing of the planar network becomes obvious, which will lead to a decrease in the training effect of the ResNet. This method simplifies difficulty and learning objectives.

In this study, Fig. 2A displayed the *Dendrobium* species identification strategy based on ResNet. Three different categories of images (plant, 1D, synchronous 2DCOS images) were divided into train set and test set, which were used as input into the ResNet model. The dataset is divided into 60 % training set, 30 % testing set and 10 % external validation set. Stochastic gradient descent (SGD) is used to update the weights and minimize the cross-entropy loss function. The ResNet models were built with the weight decay coefficient λ of 0.001 and the learning rate of 0.01. When the number of iterations or the error reaches a threshold, the optimal model is obtained. Finally, the images from the test set were fed into the trained neural network. Through forward propagation, the final identification result can be obtained. After the training set and test set are completed, external verification is required to obtain through the “confusion_matrix” code. In order to compare the influence of different neural convolutional network layers on the modeling results, we selected two convolutional layers (16 or 32) for comparison and analysis. The loss value of the model assess the convergence of the model, with a gradual decrease to a stable value (close to 0) representing a good fit. The training set accuracy evaluates the model fitting ability, the test set evaluates the model’s ability to predict new data with the same

Table 1

ResNet network parameter configuration with 16 or 32-layer convolutional neural network.

16 -layer convolutional neural network (Input image = 128×128)					
Layer name	Kernel size	Channels	Strides	Block numbers	Block name
Conv1_x	3 × 3	32	1	x1	Identity Block
Conv2_x	3 × 3	32	1	x3	Identity Block
Conv3_x	3 × 3	64	1	x1	Identity Block
	3 × 3	64	1	x1	Conv Block
Conv4_x	3 × 3	128	1	x1	Identity Block
	3 × 3	128	1	x1	Conv Block
Output Global average pooling, Flatten, Full Connection, Softmax					
32 -layer convolutional neural network (Input image = 128×128)					
Layer name	Kernel size	Channels	Strides	Block numbers	Block name
Conv1	3 × 3	32	1	x1	Identity Block
Conv2_x	3 × 3	32	1	x3	Identity Block
Conv3_x	3 × 3	64	1	x2	Identity Block
	3 × 3	64	1	x1	Conv Block
Conv4_x	3 × 3	128	1	x2	Identity Block
	3 × 3	128	1	x1	Conv Block
Conv5_x	3 × 3	256	1	x2	Identity Block
	3 × 3	256	1	x1	Conv Block
Conv6_x	3 × 3	512	1	x2	Identity Block
	3 × 3	512	1	x1	Identity Block
Output Global average pooling, Flatten, Full Connection, Softmax					

distribution, and the external validation set accuracy verifys the real scenario robustness. The Fig. 2B illustrates the structure of the ResNet model, and Fig. 2C shows the composition and number of residual modules. And the parameters configuring of 16 or 32-layer convolutional neural network are summarized in Table 1.

2.7. Support vector machines

Support vector machine is nonlinear, the algorithm transforms the original data into several support vectors through nonlinear transformation [32]. In this study, 9 species of *Dendrobium* samples can be mapped into high-dimensional space through this algorithm, and SVM can complete the identification of different kinds of *Dendrobium* samples in these high-dimensional spaces through hyperplane. The dataset is divided into 70 % training set and 30 % testing set using Kennard-Stone algorithm. The radial basis function is used to participate in the establishment of the SVM model, which is completed by coarse grid search and fine grid search. Penalty parameter (*c*) and kernel parameter (*g*) are the two main model parameters to evaluate the classification effect and validate the model performance. The *c* is used to balance the classification accuracy of the model with the complexity of the decision boundaries, where a larger model with *c* is prone to overfitting (lower fault tolerance) and too small is prone to underfitting (higher fault tolerance). The *g* is used to determine the degree of influence of the sample on the decision boundary, and *c* and *g* need to be jointly optimised. After coarse and fine parameter filtering, the best *c* and *g* were obtained. The range of two parameters in the initial grid search is set to 2^{-20} - 2^{-20} . According to the results of the initial search, the range of parameter screening is reduced and the second parameter screening is performed. The parameter results of the second screening are the best

model parameters. The process of building this model is a combination of optimal model parameters and 7-fold cross-validation.

2.8. Software

The FT-NIR spectra were preprocessed using SIMCAP⁺ 14.0 (Umetrics, Umea, Sweden). The MATLAB R2017a (MathWorks, Natick, MA, USA) was used to generate 2DCOS and build ResNet and SVM models. Other visualisation plots were done with Origin 2021 (OriginLab Corporation, Northampton, MA, USA).

3. Results and discussion

3.1. Analysis of FT-NIR spectrum

Seven characteristic peaks were observed in Fig. 3A at 8265 cm^{-1} , 6826 cm^{-1} , 5796 cm^{-1} , 5176 cm^{-1} , 4755 cm^{-1} , 4320 cm^{-1} and 4254 cm^{-1} . These absorption peaks may be caused by the high-frequency vibration of C—H, N—H, and O—H chemical bonds in the effective chemical components of polysaccharides, alkaloids, and phenols [33]. The nine *Dendrobium* species had similar absorption trends in the 9000–4400 band, with TP absorbing the highest amount of light. The TP, ZJ, HM and MG possessed two 4320 cm^{-1} and 4254 cm^{-1} absorption peaks, and CE and XY had both 4381 cm^{-1} , 4320 cm^{-1} and 4254 cm^{-1} absorption peaks. The QH, JC and GC had two absorption peaks at 4381 cm^{-1} and 4320 cm^{-1} , and the absorption was also strong at 4254 cm^{-1} , but no distinct peak was formed. After reviewing books and literatures [34–38], the spectra were resolved as follows: (1) 4000 cm^{-1} represents C—H, C—C and C—O-C combinations in polysaccharides. (2) 4386 cm^{-1} to 4252 cm^{-1} can be considered as the second overtone of C—H stretching vibration in polysaccharides. (3) Near 4750 cm^{-1} is C = O—O stretching and deformation vibration from polysaccharides. (4) Near 5172 cm^{-1} is stretching and deformation vibration of O—H, O—H stretching and first overtone of C—O deformation in water or polysaccharides. (5) The 5666 cm^{-1} is C—H from hydrocarbons or methylene. (6) The 5796 cm^{-1} is the first overtone of C—H stretching. (7) The 6830 cm^{-1} to 6784 cm^{-1} are recognized as C = O carbonyl from ketones or aldehydes. (8) Near 8258 cm^{-1} is C—H methylene from aliphatic hydrocarbons.

In order to eliminate the phenomenon that the absorption spectral lines overlap due to the mutual interference between different components of the sample, the SD method is used to process the original spectral data (Fig. 3B). It is very effective in eliminating additive and multiplicative effects in the spectrum and correcting the baseline correctly. Compared to the raw spectrum, the SD method can amplify the faint absorption peaks useful for pattern recognition models. In addition, to compare the effects of different preprocessing methods on the model, we also added SNV and MSC methods for analysis. The spectral data obtained after scattering correction in Fig. 3C and Fig. 3D Regrettably, there is no obvious difference between the spectral features after these two preprocessing. At the same time, it is difficult to distinguish different species of *Dendrobium* in all spectral bands, and these two pretreatment methods may not be suitable for identifying. This may be due to effectively eliminating the spectral differences caused by different scattering levels, thereby enhancing the correlation between the spectral data, and reducing variability between spectra.

3.2. Results of principal component analysis

PCA was used for visual analysis of different preprocessed spectral data (Figure S5) to reveal the clustering relationship among *Dendrobium* species and the effectiveness of preprocessing. The analysis based on the raw spectra (Figure S5 A) showed that the nine *Dendrobium* species overlapped together without any trend of separation. This may be due to the presence of a large amount of interfering information in the raw spectra, which masks the characteristic information. After

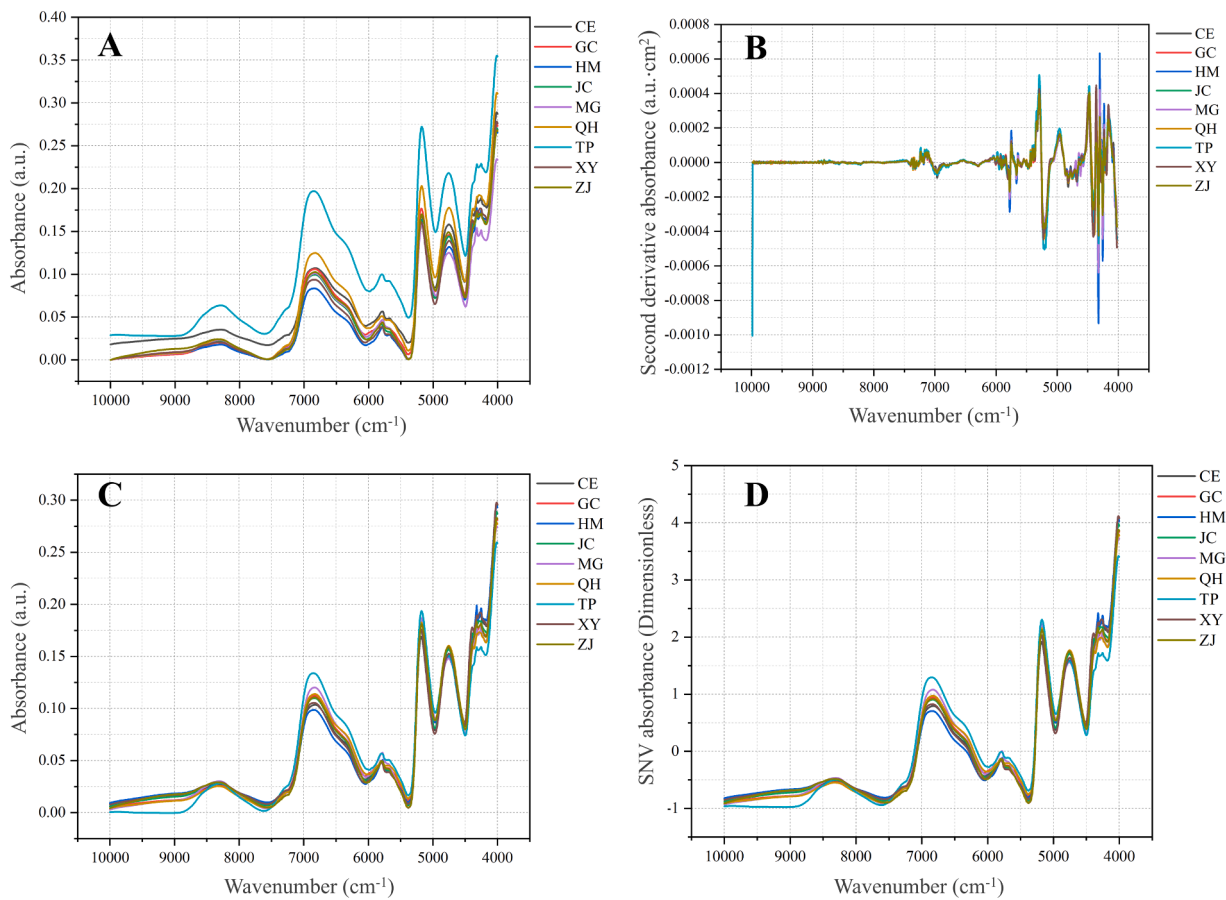


Fig. 3. Raw FT-NIR spectra and preprocessing spectra of different *Dendrobium* species. A: Raw FT-NIR spectra; B: Second-order derivatives (SD); C: Multiplicative scatter correction (MSC); D: Standard normal variate (SNV). The different coloured lines represent different *Dendrobium* species and the abbreviations of the species can be found in Table 2.

preprocessing, the differential characterization information of the nine *Dendrobium* species was obviously reflected. After SD and MSC preprocessing (Figure S5 B and C), MG was significantly separated from the other *Dendrobium* species. TP also showed a tendency to segregate from other species, but overlapped to some extent with ZJ. SNV was the worst of the preprocessing results (Figure S5 D), being only slightly better than the raw spectra. Overall, the chemical information of the nine *Dendrobium* species was very similar, and only TP and MG could show differential features after SD and MSC preprocessing. Therefore, it is necessary to extract and recognize the feature information of nine *Dendrobium* species using supervised machine learning methods.

3.3. Identification of species based on 2DCOS images

The synchronous two-dimensional correlation spectra of different species of *Dendrobium* with four preprocessing methods including raw, SD, MSC, and SNV FT-NIR spectral data were shown in Figure S6, S7, S8, and S9 respectively. 2DCOS spectra contain more important molecular structure information, greatly improving the resolution of one-dimensional spectra [39]. The synchronous 2DCOS spectrum takes the diagonal symmetry, the diagonal peaks are called auto peaks, which represent the autocorrelation of dynamic fluctuations induced by perturbation. The peaks on both sides of the diagonal are called the cross peak, which represents synchronous changes of peaks with different wave numbers. The cross-peaks located off-diagonally revealed the correlation of a pair of group vibrational intensity changes corresponding to their frequencies. The intensity peaks are called auto-peaks that appear on the diagonal and are the autocorrelation function values of the spectral intensity changes. Thence the intensity of the

autocorrelation peaks in 2DCOS is always positive. Its amplitude represents the dynamic changes of the spectral intensity during the correlation period. Therefore, in the dynamic spectrum, regions with large intensity changes show stronger autocorrelation peaks, while those regions of remain constant have minimal or no autocorrelation peaks, shows the influence of the microenvironment on functional group movement. The cross peaks are located outside the diagonal and represent the synchronous changes of the spectral signals at different wavenumbers, that the synchronized change means that there may be correlated changes or paired in spectral intensity [40].

Synchronous 2DCOS images for raw FT-NIR spectral data of different species of *Dendrobium* were displayed in Figure S6. We found that the auto-peaks are mainly distributed in the 7000–4000 cm⁻¹, indicating that the spectral information of *Dendrobium* was concentrated in this range and was connected with C—H, N—H, and O—H groups. In addition, the cross peak appeared near 6800 cm⁻¹. It can distinguish TP from other species of *Dendrobium* that there are more than three circles in the 2DCOS spectral image of TP, yet was only one or two in the other species. The appearance of cross peaks indicates it may be intramolecular or intermolecular interactions between functional groups, implying the similarity of spectral intensity changes of two corresponding frequencies. Synchronous 2DCOS images for SD FT-NIR spectral data of different species *Dendrobium* were displayed in Figure S7. Synchronous 2DCOS has better performance for visual recognition than 1D spectroscopy. Although 2DCOS overcomes these shortcomings of one-dimensional spectral peak overlap and improves its apparent resolution, it is difficult to identify other species of *Dendrobium* by visual analysis alone. The synchronous 2DCOS spectra of the MSC and SNV FT-NIR spectral data of *Dendrobium* were shown in Figure S8 and Figure S9,

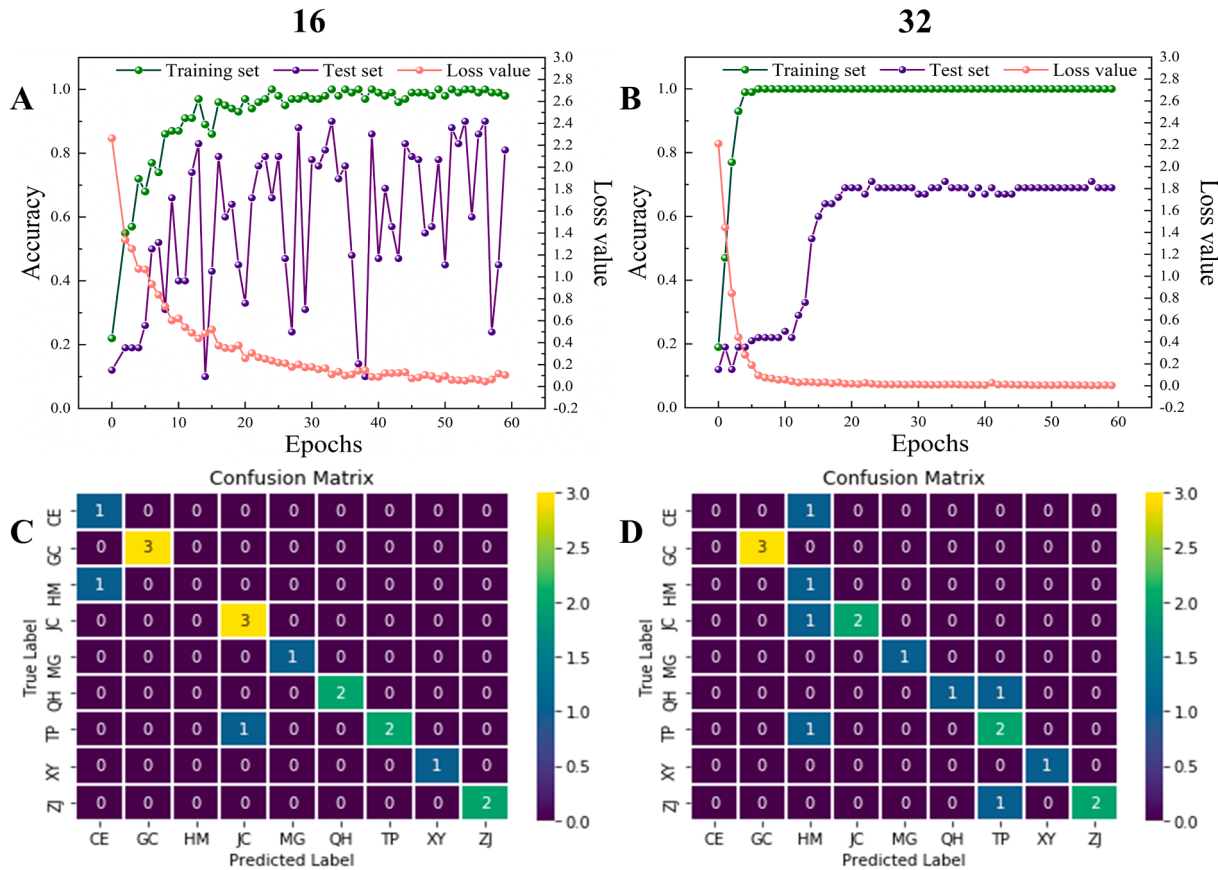


Fig. 4. The parameters of ResNet models built on plant images, with 16 convolutional layers (A and C) and 32 convolutional layers(B and D). A and B: The accuracy curves and cross-entropy cost function curves. C and D: The externally validated confusion matrix.

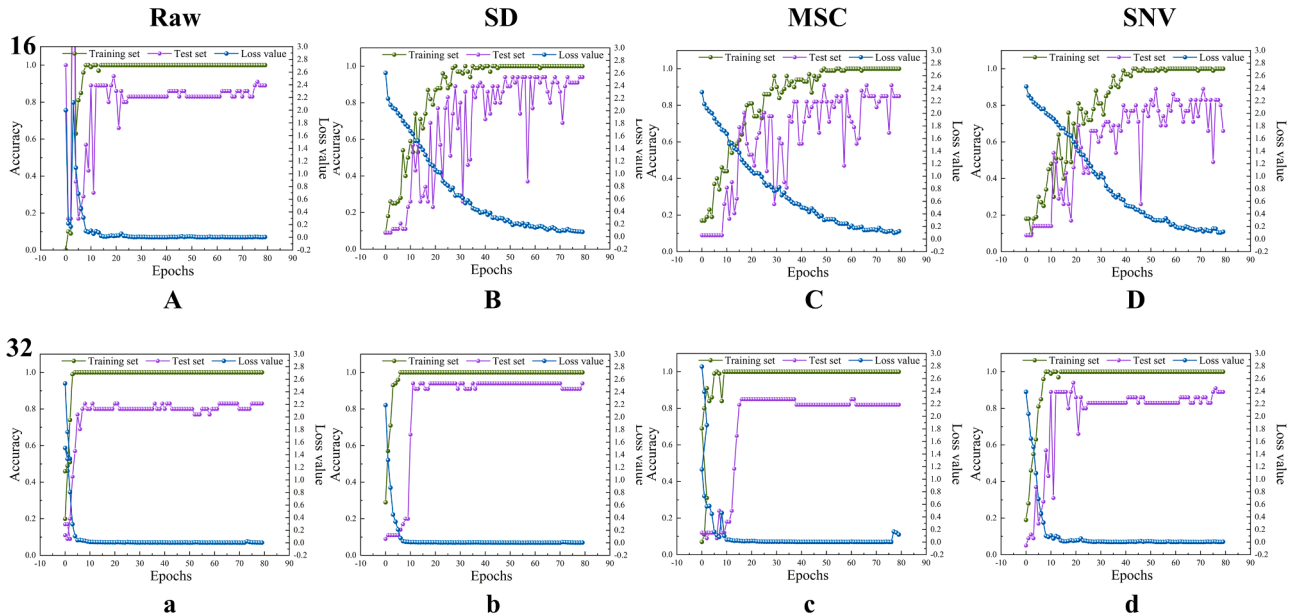


Fig. 5. The accuracy curves and cross-entropy cost function curves of ResNet models built on 1D spectral images with different preprocessing. 16 convolutional layers (A, B, C and D), 32 convolutional layers (a, b, c, and d), Raw (A and a), SD (B and b), MSC (C and c), SNV (D and d).

respectively. This result was similar to that of the raw 2DCOS images, which was a clear cross peak at 6800cm^{-1} to distinguish TP and other species of *Dendrobium*. To sum up, it is difficult to identify other species of *Dendrobium* by visual analysis alone, so it's necessary to rely on machine learning method.

3.4. Discrimination results of ResNet model with different categories images

In this model, the weight decay coefficient λ of the model is 0.0001 and the learning rate is 0.01. The ordinate is the accuracy and cost

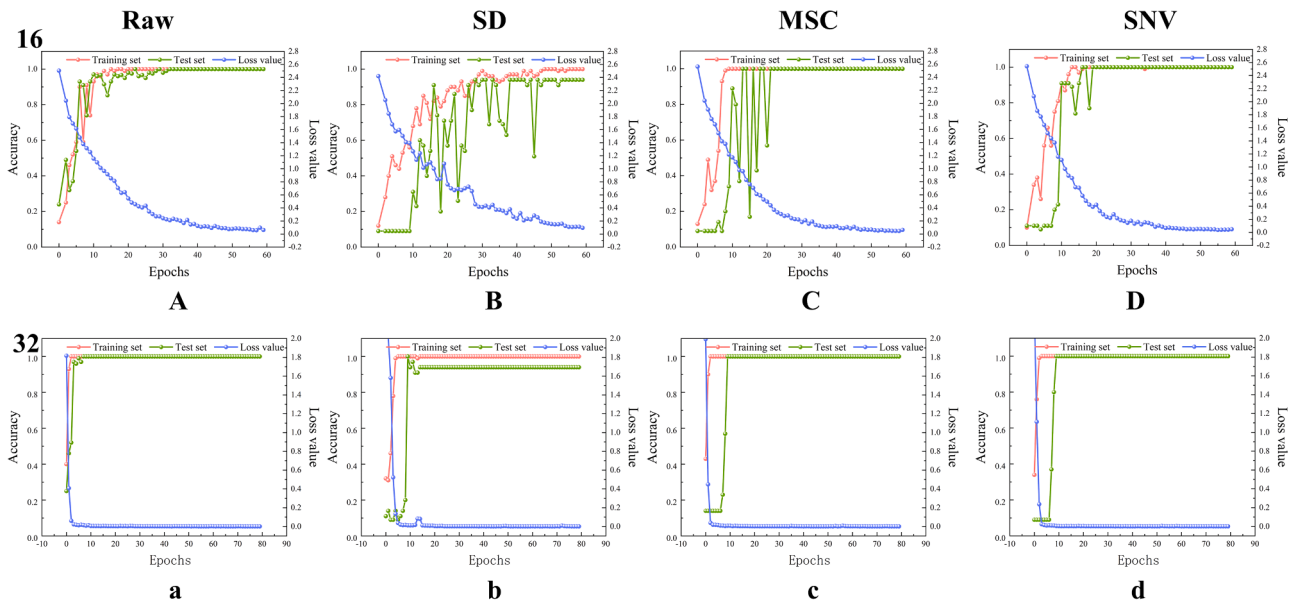


Fig. 6. The accuracy curves and cross-entropy cost function curves of ResNet models built on synchronous 2DCOS with different preprocessing. 16 convolutional layers (A, B, C and D), 32 convolutional layers (a, b, c, and d), Raw (A and a), SD (B and b), MSC (C and c), SNV (D and d).

Table 2
Detailed description of the stem morphology of 9 species of *Dendrobium*.

<i>Dendrobium</i> species	Abbreviations	Detailed description of stem morphology
<i>Dendrobium cariniferum</i>	CE	Stems fleshy and thick, cylindrical, or sometimes fusiform, with >6 nodes.
<i>Dendrobium chrysotoxum</i>	GC	Stems erect, fleshy, fusiform, with 2–5 internodes, with mostly blunt ribs, with 2–5 leaves near the top.
<i>Dendrobium williamsonii</i>	HM	Stems cylindrical, sometimes swollen and fusiform, unbranched, with several nodes
<i>Dendrobium nobile</i>	JC	Stems erect, fleshy and thick, slightly flattened cylindrical, 10–60 cm long, up to 1.3 cm thick, with many nodes, nodes sometimes slightly swollen.
<i>Dendrobium crepidatum</i>	MG	Stems hanging, fleshy, turquoise, cylindrical, unbranched, multi-noded, internodes 3–4 cm long.
<i>Dendrobium thyrsiflorum</i>	QH	Stems erect or oblique, cylindrical, thick, unbranched, with several nodes, yellowish brown and glossy, with several longitudinal edges.
<i>Dendrobium officinale</i>	TP	Stems erect, cylindrical, 9–35 cm long, 2–4 mm thick, unbranched, with many nodes.
<i>Dendrobium hancockii</i>	XY	Stems erect, hard in texture, cylindrical or sometimes fusiform with several internodes above the base, usually branched, with longitudinal grooves or ribs.
<i>Dendrobium pendulum</i>	ZJ	Stems oblique or drooping, fleshy, hypertrophic, cylindrical, unbranched, with many nodes, swollen nodes in the shape of abacus beads. Leaves are papery, oblong, apex acute, base with clasp sheaths.

function values in all curves, and the abscissa is the number of iterations. In addition, we also compared the effect of different values (16 or 32) of layer convolutional neural network on the ResNet model. The accuracy and loss values were used to evaluate the discriminative performance of this model. To compare the recognition ability of plant images, 1D images and synchronous 2DCOS of 9 *Dendrobium* species, Figs. 4, 5 and 6 were showed their modeling results, including accuracy curves and cross-entropy cost values, respectively. The loss value of all ResNet models gradually decreases to low values and remains stable, indicating that all models have good fitting and generalisation ability.

3.4.1. Plant images combined with resnet

The detailed description of plant morphological characteristics of 9 species of *Dendrobium* stems is shown in Table 2. The shape of the flower is quite different for these *Dendrobium*, but the morphological characteristics of the stem are still difficult to identify, which can be identified by the naked eye. This requires professionals with plant-related knowledge to identify the similar species of *Dendrobium*, and it is still difficult for ordinary people to distinguish different species. For example, stems of HM are cylindrical, sometimes swollen, and fusiform, up to 20 cm long, 4–6 mm thick, unbranched, with several nodes, internodes 2–3 cm long, and golden yellow when dry. This species is similar to CE, the difference is that the petals and sepals of this species are almost equal in width, the middle rib of the sepals on the back is not raised, and the ovary is not triangular. Therefore, we need to use machine learning for species identification based on plant images.

The accuracy curves and cross-entropy cost function of plant image models with different layer convolutional neural networks (16 and 32) were shown in Figs. 4A and 4B, respectively. In Fig. 4A, the train set accuracy of plant images model fluctuated up and down in the 90–100 % range, while the accuracy of the test set still fluctuates greatly, the loss value was 0.105 at 60 epochs. In Fig. 4B, the train set accuracy of plant images model was up to 100 % and the loss value was 0.095 at 6 epochs, while the test set accuracy of plant images model was up to 69 % and remain this same, the loss value was 0.014 at 24 epochs. Therefore, the layer convolutional neural network affects the results of the model that increasing the layer convolutional neural network will make the model more stable and better. The confusion matrix of the plant images models with different layer convolutional neural networks (16 and 32) were displayed in Figs. 4C and 4D, respectively. The results showed that all three images were misclassified in these types. Overall, although increasing the layer convolutional neural network will be change the stability of this model, the accuracy of the test set still cannot reach 100 %, indicating that the model based on plant images is not suitable for identifying different *Dendrobium* species. The main reason for this phenomenon that may be caused by the cluttered background of the images or the structure of the plant itself is complex, which leads to the emergence of interfering information.

3.4.2. 1D spectral images combined with resnet

The average 1D FT-NIR spectra images for different species of

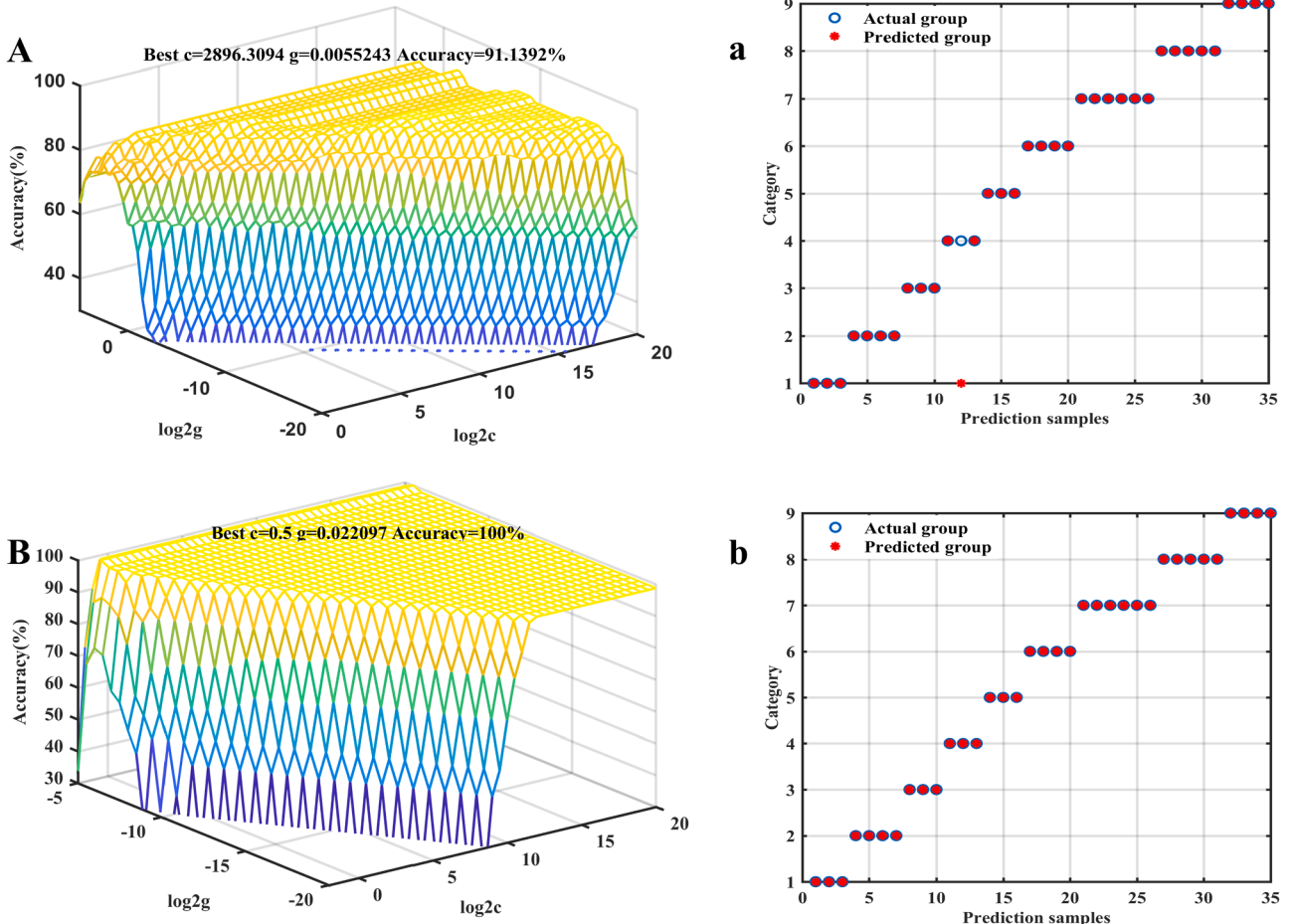


Fig. 7. The optimal separation hyperplane (A and B) and the classification results of the training set (a and b) of SVM models based on different preprocessing FT-NIR. Raw (A and a), SD (B and b).

Dendrobium based on different pretreatments were showed in Figure S2B. It can be seen that the peak shapes and peak positions of the FT-NIR spectra with different species of *Dendrobium* were similar, but their absorbance was significantly different. It indicated that different species of *Dendrobium* had different accumulation of chemical components. Compared to the other three preprocessed spectra, the SD preprocessed FT-NIR average spectrum demonstrated more subtle peaks. However, 1D average FT-NIR spectra was still difficult to identify the species of *Dendrobium* from human observations, so we need to model to analyze it.

The accuracy curves and cross-entropy cost function of 1D spectral model with different preprocessing was displayed in Fig. 5. From an overall perspective with 16-layer convolutional neural network for Fig. 5-5, the results of these models are not ideal. The number of epochs was increased to 80, the accuracy of the train set can reach 100 %, while the accuracy of the test set can reach 100 % and was up and down. From an overall perspective with 32-layer convolutional neural network for Fig. 5a, 5c, and 5d, the accuracy of the training set basically reached 100 % and remains stable when the number of epochs was <15, the loss value approaches zero, while the accuracy of the test set was about 80 %. Model results based on SD 1D images are superior and suitable for identifying different species of *Dendrobium* that the train set and test set accuracy of 1D spectral model were up to 100 % and 94 % while the loss value was 0.01 at 12 epochs. Though the loss function of the three models was all close to zero, the accuracy curve fluctuates greatly. Therefore, the stability of the model needs further verification.

The confusion matrix of 1D spectral images model with different preprocessing methods as shown in Figure S10. For these models with

16-layer convolutional neural network, it can be seen that only the spectral images in the confusion matrix of the SD 1D spectral data are fully classified correctly from the Figure S10B. There are one, two, and four 1D spectral images displayed that were misclassified for Figs. 8A, 8C, and 8D, respectively. For these models with 32-layer convolutional neural network, the classification effect of the samples has been significantly improved that only one sample in each class of confusion matrix of 1D spectral model was misclassified as shown in Figures S10a, 10c, and 10d. At the same as time, the confusion matrix of 1D spectral model with the SD preprocessed exhibited that all samples were completely correctly classified due to SD preprocessed was used to improve the spectral resolution to obtain the spectral information of the overlapping part.

Therefore, the accuracy and generalization ability of the 1D spectral image model is poor with three preprocessing methods (raw, MSC, and SNV) except SD model, and it is not suitable for the identification of *Dendrobium* species.

3.4.3. Synchronous 2DCOS spectral images combined with resnet

Based on the result of Section 3.3, the accuracy curves and cross-entropy cost function of the synchronous 2DCOS spectra on the raw, SD, MSC, and SNV were displayed in Fig. 6. Whether layer convolutional neural network is 16 or 32, the rest of the model results are superior except for the ResNet model of SD preprocessed FT-NIR spectral data, which can be used as the identification species of *Dendrobium*. In Fig. 6A, when the number of epochs was 31, the train set, test set, and loss value reached to 100 %, 100 %, and 0.211, respectively. As the number of epochs increased to 60, the loss value was 0.053. Surprisingly, in Fig. 6a,

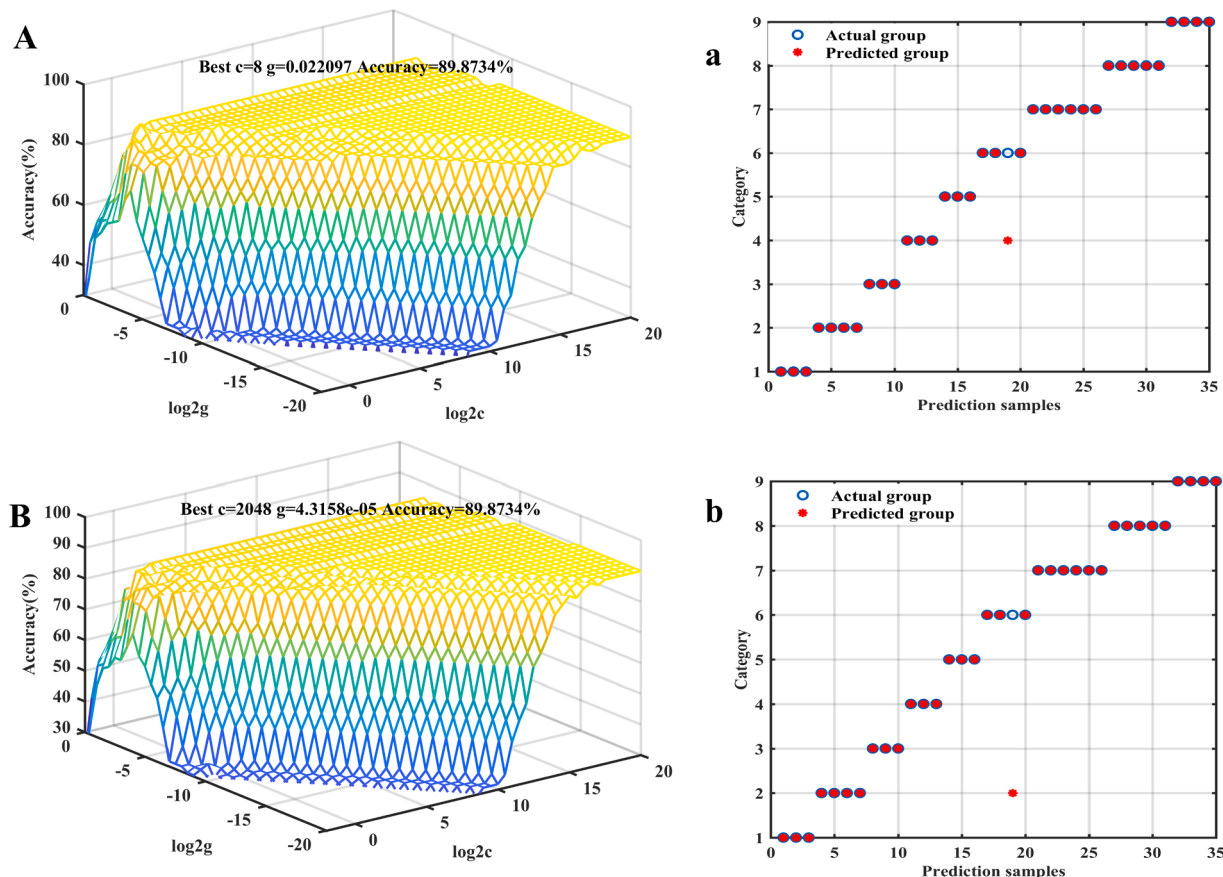


Fig. 8. The optimal separation hyperplane (A and B) and the classification results of the training set (a and b) of SVM models based on different preprocessing FT-NIR. MSC (A and a), SNV (B and b).

only the number of epochs is 7, the accuracy of both the training set and the test set reaches 100 %, and the loss value approaches 0 (0.015). Correspondingly, when the number of epochs in Fig. 6C and 6D were 17 and 18, the accuracy of train and test sets was 100 %, and the loss values were 0.59 and 0.39, respectively. Even if there is a high accuracy rate, it takes many epochs to make the loss value approach zero to ensure the robustness of the model. In Fig. 6c and Fig. 6d, only nine epochs were required, all the accuracy were 100 % and loss values approach zero (0.008 and 0.005). In a word, all FT-NIR models had 100 % accuracy of both train and test sets, slightly better than all SD FT-NIR models, it does not show its advantage in modeling recognition.

Figure S11 was the confusion matrix of synchronous 2DCOS spectra model. We can see that in Figure S11B and S11b, one spectral image belonging to QH was incorrectly classified into the XY category and the rest of the spectral images were correctly classified. This may be caused by the presence of many weak auto-peaks and cross-peaks in the SD 2DCOS spectral image. Moreover, not only were the confusion matrix of synchronous 2DCOS spectra model based on three types of preprocessing data showing a 100 % correct classification rate, but also the accuracy of train and test set were very high, indicating that its generalization ability was good and could be used as good models to identify species of *Dendrobium*.

3.5. Discrimination results of support vector machine with spectral data

In previous studies, traditional model results were poor compared to artificial intelligence (such as DL model) [41]. Therefore, in order to more objectively reflect the ability of SVM model to identify species of *Dendrobium*, we established different preprocessing SVM models to compare and analyze the FT-NIR spectral data. The optimal separation

Table 3
The SVM model parameter results based on different preprocessing.

Data types	Best c	Best g	Train set accuracy (%)	Test set accuracy (%)
Raw	2896.3094	0.0055243	91.1392	97.1429
SD	0.5	0.022097	100	100
MSC	8	0.022097	89.8734	97.1429
SNV	2048	4.3158e-05	89.8734	97.1429

hyperplane and the classification results of the training set of SVM models based on different preprocessing FT-NIR were showed in the Fig. 7 and 8. The SVM model parameter results based on different preprocessing was displayed in Table 3. All models showed similar performance, but the train and test set accuracy showed slight differences, and the magnitude of the model parameter values varies greatly. It is worth noting that the accuracy rates of the train set and test set based on the SD model are both 100 % and had a lower value of best c and g (0.5 and 0.022097), indicating that this model can accurately identify different species of *Dendrobium*. Secondly, the model with better performance is MSC. The accuracy of the train set and the test set, the best c , and g values were 89.9734 %, 97.1429 %, 8, and 0.022097, respectively. However, even though the original and SNV dataset models have high accuracy, they had high the best c values (2896.3094 and 2048), indicating the model had high error tolerance and poor robustness, which was not suitable for species identification of *Dendrobium*. The Figs. 7 (a, b) and 8 (a, b) clearly showed the classification of the test set. All of them are classified correctly after SD preprocessing, and the rest of the datasets have one sample misclassified. The higher the value of parameter c , the fault tolerance of the model was the higher. Three-dimensional score

Table 4

The discrimination results of FT-NIR spectra model based on different processing.

Image types	Preprocessing methods	Epochs	Number of convolutional layers	Accuracy (%)			Loss value	Training Time (s)
				Train set	Test set	External validation set		
Plant images	–	60	16	0.98	0.81	88.2	0.105	105.4
	–	60	32	1	0.69	76.5	0.004	110.5
1D images	Raw	80	16	1	0.71	90.9	0.12	22.8
	SD	80	16	1	0.94	100	0.073	24
	MSC	80	16	1	0.85	81.8	0.126	21.9
	SNV	80	16	1	0.66	72.7	0.117	24.1
	Raw	80	32	1	0.80	90.9	0.005	26.2
	SD	80	32	1	0.94	100	0.003	33.3
2DCOS images	MSC	80	32	1	0.82	90.9	0.002	32.4
	SNV	80	32	1	0.89	90.9	0.005	25.8
	Raw	80	16	1	1	100	0.053	5.4
	SD	80	16	1	0.94	90.9	0.085	6.9
	MSC	80	16	1	1	100	0.054	7.1
	SNV	80	16	1	1	100	0.029	7.9
2DCOS images	Raw	80	32	1	1	100	0.001	11.5
	SD	80	32	1	0.94	90.9	0.001	14.1
	MSC	80	32	1	1	100	0.001	11.1
	SNV	80	32	1	1	100	0.000	17.3

plots for each parameter combination for each spectrum showed different accuracy rates under 7-fold cross-validation. Under the premise of the same train set and test set accuracy, the penalty parameter was lower, indicating that the model was more robust. Therefore, the best SVM model based on SD preprocessed FT-NIR datasets was also beneficial for the identification of different species of *Dendrobium*.

3.6. Compare different authentication models

The Table 4 presents the discrimination results of FT-NIR spectra models based on different image types (plant images, 1D, and 2DCOS images) with different processing. The 16 and 32-layer convolutional neural network model of synchronous 2DCOS on the raw and pretreated with MSC and SNV spectra has 100 % accuracy of the train set, test set and external validation set. The results reveal that the model has strong stability and generalization ability. The models on 1D and 2DCOS images with preprocessed SD comes next. Their train set accuracy are 100 %, test set accuracy is 94 %, and external validation set accuracy are 100 % and 90.9 %. These models have high accuracy and generalization ability, and can be used to determine different species of *Dendrobium*. In addition, we find that when the number of convolutional layers is 16, the training time is relatively short, which can save running time and improve the discrimination efficiency. The rest of the models have 100 % accuracy on the training set, but have lower accuracy on the test set and external validation set, and their generalization ability is poor, so the model is unreliable to species identification of *Dendrobium*. Moreover, we found that increasing the number of convolutional layers not only did not significantly improve the model accuracy, but also increased the running time.

On the basis of these results, we conclude that the models on 2DCOS images are superior than plant images and 1D images. Among them, the remaining three models (raw, MSC, and SNV) except the model based on SD 2DCOS images are better. It may be because the color information of these three types spectra is more abundant, and their automatic peaks and cross-peaks is clearer, which is often used to improve spectral resolution. On the contrary, the model based on SD preprocessed 1D images is good. This may be related to the fact that the derivative algorithm can eliminate the interference caused by baseline drift or flat background, resolve overlapping peaks, improve resolution and sensitivity. In a 1D dynamic spectrum, two absorption peaks that are too close together to overlap, if they are from different functional groups, may appear as two distinct independent peaks in a 2DCOS. It is regrettable that the accuracy of the test set modeled directly with plant images of *Dendrobium* stems is low (81 % and 69 %), the training time is long, and the time

required for each iteration is about 105 s. This may not apply to the identification of different species of *Dendrobium* in this work. But it is worth affirming that the identification species of *Dendrobium* based on plant images can reduce the damage of plant physiological characteristics. And with the development of hyperspectral imaging sensors, rapid, non-invasive, and non-destructive measurements of plant physiological states have become feasible [42]. Therefore, it is necessary to collect the stems of the plants in the laboratory to take pictures for modeling, and exclude the interference factors of other parts of *Dendrobium* in the future research.

Moreover, we found that the SD-preprocessed FT-NIR spectral data information is also directly used for SVM modeling, which can be used for species identification of *Dendrobium*. Compared with artificial intelligence technologies (such as ResNet), this model may have the disadvantage of being time-consuming when using large samples that it takes hours or even half a day to build a model. It showed that the SVM model may be more suitable for the identification of small samples, while the ResNet model based on the synchronous 2DCOS spectral images with no preprocessing is more suitable for the species identification of large samples of *Dendrobium*, which reduces the complexity of data processing and the time cost of analyzing spectral data. The above research results can provide feasible, efficient, and optional methods to solve the confusion of similar species in agriculture or other fields.

4. Conclusion

This study successfully established a new method for authenticating *Dendrobium* species, which is non-destructive and fast. Simultaneous authentication of photographic identity and chemical information from the genus *Dendrobium*. For the ResNet model, the synchronous 2DCOS dataset performs the best, extracting more useful recognition information than one-dimensional FT-NIR spectral and plant images datasets. Preprocessing is generally useful for correcting and displaying FT-NIR spectral features, but our study found that choosing the right preprocessing method is very important. For one-dimensional spectra, SD preprocessing is the most effective, but for synchronous 2DCOS, SD processing is counterproductive. Compared with SVM models, ResNet models have higher accuracy and recognition speed, and the spectral data can reach 100 % without preprocessing. The recognition accuracy based on plant images is 88.2 %, which is not as good as other datasets. It is recommended to use flower parts with more recognized features in the future. This study may provide new ideas for identifying similar species, genuine and fake products, pest and disease characteristics in agricultural problems.

Funding

This work was supported by the Special Program for the Major Science and Technology Projects of Yunnan Province (Grant number: 202202AE090001), the Key Industrial Science and Technology Projects Served by Yunnan Province's Universities (Grant number: FWCY-BSPY2025015), and the Scientific Research and Innovation Project of Postgraduate Students in the Academic Degree of YunNan University (Grant number: KC23235459).

Ethics statement

Not applicable: This manuscript does not include human or animal research.

CRediT authorship contribution statement

Yulin Xu: Writing – review & editing, Writing – original draft, Software, Methodology, Investigation, Formal analysis. **Lian Li:** Writing – review & editing, Writing – original draft, Software, Methodology, Formal analysis, Data curation. **Yuanzhong Wang:** Validation, Supervision, Project administration, Conceptualization. **Qiang Hu:** Supervision.

Declaration of competing interest

The authors declare that they have no known competing financial interests or personal relationships that could have appeared to influence the work reported in this study.

Supplementary materials

Supplementary material associated with this article can be found, in the online version, at [doi:10.1016/j.atech.2025.101027](https://doi.org/10.1016/j.atech.2025.101027).

Data availability

Data will be made available on request.

References

- [1] Z. Wang, M. Zhao, H. Cui, J. Li, M. Wang, Transcriptomic landscape of medicinal *dendrobium* reveals genes associated with the biosynthesis of bioactive components, *Front Plant Sci* 11 (2020) 391, <https://doi.org/10.3389/fpls.2020.00391>.
- [2] X. Xing, S.W. Cui, S. Nie, G.O. Phillips, H.Douglas Goff, Q. Wang, A review of isolation process, structural characteristics, and bioactivities of water-soluble polysaccharides from *Dendrobium* plants, *Bioact. Carbohydr. Diet. Fibre* 1 (2013) 131–147, <https://doi.org/10.1016/j.bcd.2013.04.001>.
- [3] X. Gu, S. Zhu, H. Du, C. Bai, X. Duan, Y. Li, K. Hu, Comprehensive multi-component analysis for authentication and differentiation of 6 *dendrobium* species by 2D NMR-based metabolomic profiling, *Microchem J* 176 (2022) 107225, <https://doi.org/10.1016/j.microc.2022.107225>.
- [4] Y. Lam, T.B. Ng, R.M. Yao, J. Shi, K. Xu, S.C. Sze, K.Y. Zhang, Evaluation of chemical constituents and important mechanism of pharmacological biology in *Dendrobium* plants, *Evid Based Complement Altern. Med* (2015) 841752, <https://doi.org/10.1155/2015/841752>, 2015.
- [5] M. Kamruzzaman, Y. Makino, S. Oshita, Non-invasive analytical technology for the detection of contamination, adulteration, and authenticity of meat, poultry, and fish: a review, *Anal Chim Acta* 853 (2015) 19–29, <https://doi.org/10.1016/j.aca.2014.08.043>.
- [6] K.B. Walsh, V.A. McGlone, D.H. Han, The uses of near infra-red spectroscopy in postharvest decision support: a review, *Postharvest Biol Tec* 163 (2020), <https://doi.org/10.1016/j.postharvbio.2020.111139>.
- [7] M. Jimenez-Hernandez, M.D. Brown, C. Hughes, N.W. Clarke, P. Gardner, Characterising cytotoxic agent action as a function of the cell cycle using fourier transform infrared microspectroscopy, *Analyst* 140 (2015) 4453–4464, <https://doi.org/10.1039/c5an00671f>.
- [8] Y.G. Ding, Q.Z. Zhang, Y.Z. Wang, A fast and effective way for authentication of *dendrobium* species: 2DCOS combined with ResNet based on feature bands extracted by spectrum standard deviation, *Spectrochim Acta Mol Biomol Spectrosc* 261 (2021) 120070, <https://doi.org/10.1016/j.saa.2021.120070>.
- [9] L. Li, Y. Zhao, Z. Li, Y. Wang, Multi-information based on ATR-FTIR and FT-NIR for identification and evaluation for different parts and harvest time of *dendrobium officinale* with chemometrics, *Microchem J* 178 (2022) 107430, <https://doi.org/10.1016/j.microc.2022.107430>.
- [10] W. Xie, J. Lei, J. Yang, Y. Li, Q. Du, Z. Li, Deep latent spectral representation learning-based hyperspectral band selection for target detection, *IEEE Trans. Geosci. Remote Sens.* 58 (2020) 2015–2026, <https://doi.org/10.1109/tgrs.2019.2952091>.
- [11] S.S. Virnodkar, V.K. Pachghare, V.C. Patil, S.K. Jha, Remote sensing and machine learning for crop water stress determination in various crops: a critical review, *Precis Agric* 21 (2020) 1121–1155, <https://doi.org/10.1007/s11119-020-09711-9>.
- [12] T. Jiang, X.J. Wang, Hyperspectral images classification based on fusion features derived from 1d and 2d convolutional Neural network, *The international archives of the photogrammetry, Remote Sens. Spat. Inform. Sci.* XLII-3/W10 (2020) 335–341, <https://doi.org/10.5194/isprs-archives-XLII-3-W10-335-2020>.
- [13] A. Khan, A.D. Vibhute, S. Mali, C.H. Patil, A systematic review on hyperspectral imaging technology with a machine and deep learning methodology for agricultural applications, *Ecol Inf.* 69 (2022) 101678, <https://doi.org/10.1016/j.ecoinf.2022.101678>.
- [14] F. Arias, M. Zambrano, K. Broce, C. Medina, H. Pacheco, Y. Nunez, Hyperspectral imaging for rice cultivation: applications, methods and challenges, *Aims. Agric. Food* 6 (2021) 273–307, <https://doi.org/10.3934/agrfood.2021018>.
- [15] K. He, S. Ren, X. Zhang, J. Sun, Deep residual learning for image recognition, 2016, pp. 770–778, <https://doi.org/10.1109/CVPR.2016.90>.
- [16] J. Jiao, W.-C. Tu, S. He, R.W.H. Lau, FormResNet: formattted residual Learning for image restoration, in: 2017 IEEE Conference on Computer Vision and Pattern Recognition Workshops (CVPRW), 2017, pp. 1034–1042, <https://doi.org/10.1109/cvprw.2017.140>.
- [17] Y. LeCun, G. Bengio, G. Hinton, Deep learning, *Nature* 521 (2015) 436–444, <https://doi.org/10.1038/nature14539>.
- [18] S.D. Krauss, R. Roy, H.K. Yosef, T. Lechtenen, S.F. El-Mashtoly, K. Gerwert, A. Mosig, Hierarchical deep convolutional neural networks combine spectral and spatial information for highly accurate Raman-microscopy-based cytopathology, *J Biophotonics* 11 (2018) e201800022, <https://doi.org/10.1002/jbio.201800022>.
- [19] R. Akter, M.I. Hosen, CNN-based leaf image classification for Bangladeshi medicinal plant recognition, 2020 Emerging Technology in Computing, Communication and Electronics (ETCCE), 2020, pp. 1–6, <https://doi.org/10.1109/etcce51779.2020.9350900>.
- [20] J.E. Dong, J. Zhang, Z.T. Zuo, Y.Z. Wang, Deep learning for species identification of bolete mushrooms with two-dimensional correlation spectral (2DCOS) images, *Spectrochim Acta Mol Biomol Spectrosc* 249 (2021) 119211, <https://doi.org/10.1016/j.saa.2020.119211>.
- [21] Z. Liu, S. Yang, Y. Wang, J. Zhang, Discrimination of the fruits of *Amomum tsao-ko* according to geographical origin by 2DCOS image with RGB and resnet image analysis techniques, *Microchem J* 169 (2021) 106545, <https://doi.org/10.1016/j.microc.2021.106545>.
- [22] J.-E. Dong, S. Zhang, T. Li, Y.-Z. Wang, 2DCOS combined with CNN and blockchain to trace the species of boletes, *Microchem J* 177 (2022) 107260, <https://doi.org/10.1016/j.microc.2022.107260>.
- [23] F. Jiang, Y. Lu, Y. Chen, D. Cai, G. Li, Image recognition of four rice leaf diseases based on deep learning and support vector machine, *Comput Electron Agr* 179 (2020) 105824, <https://doi.org/10.1016/j.compag.2020.105824>.
- [24] A. Gopal, S.P. Reddy, V. Gayatri, Classification of selected medicinal plants leaf using image processing, 2012, pp. 5–8, <https://doi.org/10.1109/MVIP.2012.6428747>.
- [25] Å. Rinnan, F.v.d. Berg, S.B. Engelsen, Review of the most common pre-processing techniques for near-infrared spectra, *Trac-Trend Anal Chem* 28 (2009) 1201–1222, <https://doi.org/10.1016/j.trac.2009.07.007>.
- [26] N. I., Two-dimensional infrared (2D IR) spectroscopy: theory and applications, *Appl Spectrosc* 44 (1990) 550–561, <https://doi.org/10.1366/0003702904087398>.
- [27] R.-J. Yang, C.-Y. Liu, Y.-R. Yang, H.-Y. Wu, H. Jin, H.-Y. Shan, H. Liu, Two-trace two-dimensional(2T2D) correlation spectroscopy application in food safety: a review, *J Mol Struct* 1214 (2020) 128219, <https://doi.org/10.1016/j.molstruc.2020.128219>.
- [28] R. Yang, G. Dong, X. Sun, Y. Yu, H. Liu, Y. Yang, W. Zhang, Synchronous-asynchronous two-dimensional correlation spectroscopy for the discrimination of adulterated milk, *Anal Methods-Uk* 7 (2015) 4302–4307, <https://doi.org/10.1039/c5ay00134j>.
- [29] R. Yang, R. Liu, X. Kexin, Detection of adulterated milk using two-dimensional correlation spectroscopy combined with multi-way partial least squares, *Food Biosci* 2 (2013) 61–67, <https://doi.org/10.1016/j.fbio.2013.04.005>.
- [30] R. Yang, Y. Yang, G. Dong, W. Zhang, Y. Yu, Multivariate methods for the identification of adulterated milk based on two-dimensional infrared correlation spectroscopy, *Anal Methods-Uk* 6 (2014), <https://doi.org/10.1039/c4ay00442f>, 3461–3441.
- [31] Z. Wu, C. Shen, A. van den Hengel, Wider or deeper: revisiting the ResNet model for visual recognition, *pattern recogn.* 90 (2019) 119–133, <https://doi.org/10.1016/j.patcog.2019.01.006>.
- [32] S. Mahadevan, S.L. Shah, T.J. Marrie, C.M. Slupsky, Analysis of metabolomic data using support vector machines, *Anal Chem* 80 (2008) 7562–7570, <https://doi.org/10.1021/ac800954c>.
- [33] T.B. Ng, J. Liu, J.H. Wong, X. Ye, S.C. Wing Sze, Y. Tong, K.Y. Zhang, Review of research on *Dendrobium*, a prized folk medicine, *Appl Microbiol Biotechnol* 93 (2012) 1795–1803, <https://doi.org/10.1007/s00253-011-3829-7>.
- [34] L. Ma, Z. Zhang, X. Zhao, S. Zhang, H. Lu, The rapid determination of total polyphenols content and antioxidant activity in *dendrobium officinale* using near-

- infrared spectroscopy, *Anal Methods-Uk* 8 (2016) 4584–4589, <https://doi.org/10.1039/c6ay00542j>.
- [35] Y. Wei, W. Fan, X. Zhao, W. Wu, H. Lu, Rapid authentication of *dendrobium officinale* by near-infrared reflectance spectroscopy and chemometrics, *Anal Lett* 48 (2014) 817–829, <https://doi.org/10.1080/00032719.2014.963595>.
- [36] J. Xu, Q.-B. Han, S.-L. Li, X.-J. Chen, X.-N. Wang, Z.-Z. Zhao, H.-B. Chen, Chemistry, bioactivity and quality control of *Dendrobium*, a commonly used tonic herb in traditional Chinese medicine, *Phytochem Rev* 12 (2013) 341–367, <https://doi.org/10.1007/s11101-013-9310-8>.
- [37] M.G. López, A.S. García-González, E. Franco-Robles, Carbohydrate analysis by NIRS-Chemometrics, 2017 chapter 4, <https://www.10.5772/67208>.
- [38] E.W. Ciurczak, B. Igne, J. Workman, D.A. Burns, Handbook of Near-Infrared analysis, 2021. <https://www.10.1201/b22513>.
- [39] J. Chen, Y. Wang, L. Rong, J. Wang, Integrative two-dimensional correlation spectroscopy (i2DCOS) for the intuitive identification of adulterated herbal materials, *J Mol Struct* 1163 (2018) 327–335, <https://doi.org/10.1016/j.molstruc.2018.02.061>.
- [40] Q.W. Wu, J. two dimensional correlation analytic spectroscopy, *Huaxue Tongbao* 63 (2000) 45–53, <https://doi.org/10.14159/j.cnki.0441-3776.2000.08.012>.
- [41] L. Wang, J. Li, T. Li, H. Liu, Y. Wang, Method superior to traditional spectral identification: FT-NIR two-dimensional correlation spectroscopy combined with deep learning to identify the shelf life of fresh *Phlebopus portentosus*, *ACS Omega* 6 (2021) 19665–19674, <https://doi.org/10.1021/acsomega.1c02317>.
- [42] M.S. Mohd Asaari, S. Mertens, L. Verbraeken, S. Dhondt, D. Inzé, K. Bikram, P. Scheunders, Non-destructive analysis of plant physiological traits using hyperspectral imaging: a case study on drought stress, *Comput Electron Agr* 195 (2022) 106808, <https://doi.org/10.1016/j.compag.2022.106806>.